Backbone Dynamics of Reduced Plastocyanin from the Cyanobacterium *Anabaena variabilis*: Regions Involved in Electron Transfer Have Enhanced Mobility[†,‡]

Lixin Ma,[§,||] Mathias A. S. Hass,[§] Nanna Vierick,[§] Søren M. Kristensen,[§] Jens Ulstrup,[⊥] and Jens J. Led*[,§]

Department of Chemistry, University of Copenhagen, Universitetsparken 5, DK-2100 Copenhagen Ø, Denmark, and Chemistry Department, The Technical University of Denmark, Building 207, DK-2800 Lyngby, Denmark

Received August 26, 2002; Revised Manuscript Received November 11, 2002

ABSTRACT: The dynamics of the backbone of the electron-transfer protein plastocyanin from the cyanobacterium *Anabaena variabilis* were determined from the ^{15}N and $^{13}C^{\alpha}$ R_1 and R_2 relaxation rates and steady-state [^{1}H]−^{15}N and [^{1}H]−^{13}C nuclear Overhauser effects (NOEs) using the model-free approach. The ^{13}C relaxation studies were performed using ^{13}C in natural abundance. Overall, it is found that the protein backbone is rigid. However, the regions that are important for the function of the protein show moderate mobility primarily on the microsecond to millisecond time scale. These regions are the "northern" hydrophobic site close to the metal site, the metal site itself, and the "eastern" face of the molecule. In particular, the mobility of the latter region is interesting in light of recent findings indicating that residues also on the eastern face of plastocyanins from prokaryotes are important for the function of the protein. The study also demonstrates that relaxation rates and NOEs of the $^{13}C^{\alpha}$ nuclei of proteins are valuable supplements to the conventional ^{15}N relaxation measurements in studies of protein backbone dynamics.

Proteins perform motions over a wide frequency range, from small-amplitude backbone fluctuations and side-chain motions on the picosecond time scale, over concerted motions of flexible loops on the microsecond to millisecond time scale, to large rearrangements of domains that can take hours or weeks. These movements at the molecular level are essential for the function of proteins, as demonstrated by numerous studies in recent years (*1*−*6*). A combined study of the structure and dynamics of biomacromolecules is therefore necessary for obtaining a detailed description of their function.

NMR[1] relaxation measurements (*7*−*9*) provide a powerful tool for mapping intramolecular mobility of proteins in solution (*10*−*12*). This method can give information about both fast motion on the picosecond to nanosecond time scale and slower motion on the microsecond to millisecond time scale, including chemical exchange. Usually, the approach includes the determination of the relaxation parameters R_1 and R_2 and the nuclear Overhauser effect (NOE) of the backbone amide ^{15}N nuclei, using isotopically labeled samples. Also, relaxation of the ^{13}C nuclei can be used, enabling studies of the dynamics of the side chains. However, in uniformly ^{13}C-enriched samples, the ^{13}C−^{13}C scalar couplings make it unfeasible to measure the relaxation rates accurately (*13*), except for the carbonyl ^{13}C nuclei (*14*). Yet the relaxation parameters can be obtained from ^{13}C in randomly enriched samples (*15*), or even from samples with ^{13}C in natural abundance (*16*, *17*).

Here, we have studied the backbone dynamics of the electron-transfer protein plastocyanin from the cyanobacterium *Anabaena variabilis* to gain further insight into the mechanism of the electron-transfer process. The studies are based on the relaxation rates and NOEs of the amide ^{15}N and $^{13}C^{\alpha}$ nuclei using a ^{15}N-enriched sample of the protein and samples with ^{13}C in natural abundance.

Plastocyanin (PCu) is a 10.5 kDa type I blue copper protein. It is involved in the electron transport between the two membrane-embedded protein complexes, cytochrome b_6f and P700 of photosystem I (PSI) in all higher plants, green algae, and some photosynthetic bacteria among these cyanobacteria (blue-green algae) (*18*−*20*). PCu is a water-soluble protein. In higher plants and green algae, it is present on the lumen side of the thylakoid membrane of the

[†] This work was financially supported by the Danish Natural Science Research Council (9400351, 9502759, 9801801, and 51-00211), Lundbeckfonden, Carlsbergfondet, and Novo Nordisk Fonden.

[‡] The ^{15}N and $^{13}C^{\alpha}$ R_1 and R_2 relaxation and NOE data and the assigned ^{15}N, $^{13}C^{\alpha}$, and ^{1}H chemical shifts of *A.v.* PCu have been deposited in the BioMagResBank (http://www.bmrb.wisc.edu) under BMRB accession number 5505.

* To whom correspondence should be addressed: Department of Chemistry, University of Copenhagen, Universitetsparken 5, DK-2100 Copenhagen Ø, Denmark, Telephone: (+45) 3532 0302. Fax: (+45) 3535 0609. E-mail: led@kiku.dk.

[§] University of Copenhagen.

[||] Present address: Department of Medicinal Chemistry, Purdue University, West Lafayette, IN 47907.

[⊥] The Technical University of Denmark.

[1] Abbreviations: *A.v.* PCu, *Anabaena variabilis* plastocyanin; CPMG, Carr−Purcell−Meiboom−Gill; CSI, chemical shift index; Cyt *f*, cytochrome *f*; GARP, globally optimized alternating-phase rectangular pulses; HMQC-COSY, heteronuclear multiple-quantum correlation, correlated spectroscopy; HNCA, experimental scheme correlating ^1H_i and $^{15}N_i$ with $^{13}C^{\alpha}_i$ and $^{13}C^{\alpha}_{i-1}$; HNCO, experimental scheme correlating ^1H_i, $^{15}N_i$, and $^{13}C'_{i-1}$; HSQC, heteronuclear single-quantum coherence; HSQC-TOCSY, heteronuclear single-quantum coherence, total correlation spectroscopy; LSQ, least-squares fitting; NMR, nuclear magnetic resonance; NOE, nuclear Overhauser effect; NOESY, NOE spectroscopy; PAC, perturbed angular correlation; PSI, photosystem I; TPPI, time-proportional phase increments; rmsd, root-mean-square deviation; SD, standard deviation.

10.1021/bi020553h CCC: $25.00
Published on Web 12/20/2002

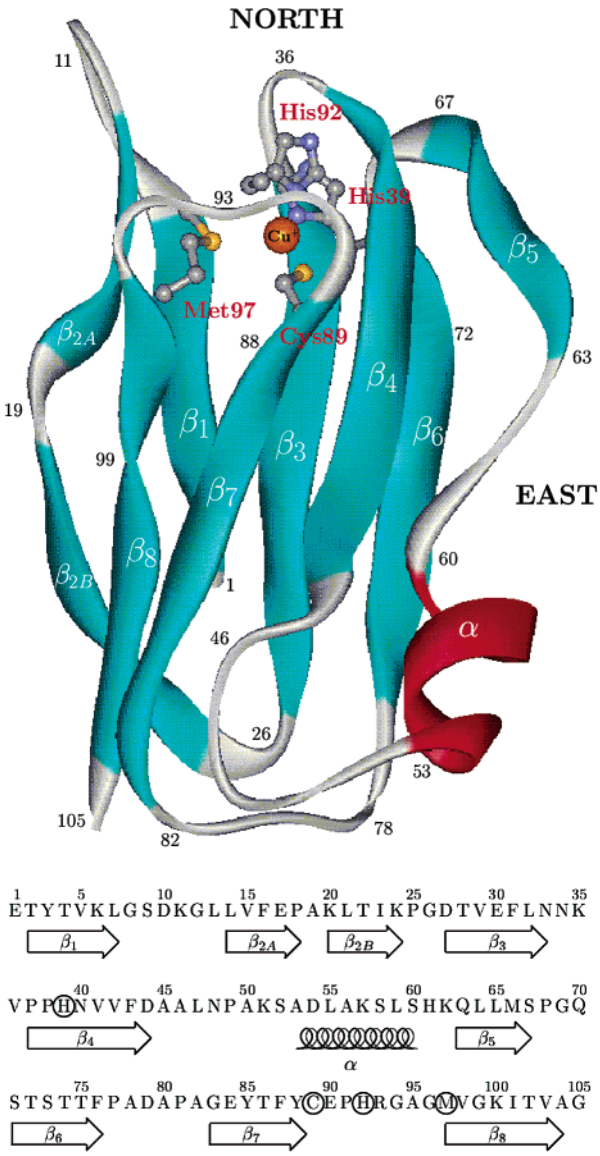

FIGURE 1: Schematic representation of the energy-minimized average solution structure of *A.v.* PCu (PDB entry 1FA4) (*26*) and the amino acid sequence and secondary structure elements of *A.v.* PCu. Blue indicates β-strand and red α-helix. The four copper binding residues are encircled in the sequence, and their side chains are shown as balls and sticks in the structure.

chloroplast and in prokaryotes in the corresponding periplasmic space between the plasma membrane and the outer membrane.

As a type I blue copper protein, PCu has its copper ion bound to four ligands in a distorted tetrahedral configuration. The four ligands are two histidines, one cysteine, and one weakly bound methionine. The structures of plastocyanins from a variety of organisms have been determined using X-ray crystallography and NMR spectroscopy. This includes the structures of five different plastocyanins from cyanobacteria (*21*−*26*). One of these is the NMR structure of plastocyanin from *A. variabilis* (*A.v.* PCu) (*25*, *26*), a 105-residue plastocyanin (Figure 1). Among the residues of *A.v.* PCu, 65 are conserved in PCu from the cyanobacterium *Phormidium laminosum* and 42 in poplar PCu. The residue numbering used here is that of *A.v.* PCu, while the corresponding numbers of poplar PCu are given in brackets.

For plastocyanin from eukaryotes, extensive studies have been made of the electron transfer mechanism of plastocyanins from higher plants. These studies, mainly kinetic measurements and mutation studies, have revealed two regions on the surface of PCu that are crucial for binding and electron transfer to PSI and from cytochrome *f* (Cyt *f*), the subunit of cytochrome b_6f that reacts with PCu. The contact surface between PCu from spinach and Cyt *f* from turnip was recently mapped using NMR spectroscopy (*27*). A strongly negatively charged region rather distant from the copper center (10−15 Å) termed the "east site", the acidic patch or the remote site, is responsible for the initial binding to Cyt *f* and PSI (*28*). The east site consists of two regions called the large and small acidic patch located on each side of Tyr88(83). Kinetic studies (*29*) and computer simulations (*30*) show that the complex rearranges after the initial binding of PCu to Cyt *f*. As a result of the rearrangement, the second important region, a flat hydrophobic surface close to the copper ion termed the "north site", the adjacent site or the hydrophobic patch, comes into contact with the acceptor or donor protein. This brings the two redox centers within ∼15 Å of each other, and provides a favorable configuration for electron transfer. A similar mechanism has been proposed for the interaction with PSI (*18*, *31*−*35*). Electron transfer is thought to occur mainly from the surface-exposed copper ligand His92(87). Electron transfer via Tyr88(83) on the east site can be made to act as an alternative pathway (*36*, *37*), but so far there is no evidence that this pathway should be important in biological systems.

For plastocyanins from prokaryotes, the most striking difference between prokaryotic and eukaryotic plastocyanins is the difference in their electrostatic surface potentials. Whereas the overall charge of plastocyanins in higher plants is negative (approximately −9), prokaryotic plastocyanins are close to neutral and can even be positive. This is because prokaryotic plastocyanins lack most of the negatively charged residues at the east site, and some are even replaced with positively charged residues. In *A.v.* plastocyanin, the east site is slightly positively charged as is the overall charge of the protein, resulting in an isoelectric point of 8.4 (*38*). This suggests that in prokaryotes the binding of PCu to PSI and Cyt *f* is accomplished by different means. NMR investigations using intermolecular chemical shift perturbations, in combination with molecular dynamics simulations, suggest that the east site does not make contact with Cyt *f* (*39*), at least not in a well-defined complex. Still, recent site-directed mutagenesis studies (*40*) show that mutations of charged residues on the east site do affect the reactivity, suggesting also that the east site is involved in complex formation. This suggestion has recently been substantiated by intermolecular paramagnetic relaxation studies of *A.v.* plastocyanin (*41*), indicating that the eastern face of *A.v.* PCu participates in an intermolecular contact. Also of interest in this context is the suggestion that in prokaryotic systems, opposite eukaryotic systems, *positively* charged residues on the east site are important for binding through electrostatic interaction with *negatively* charged residues in Cyt *f* (*42*) and PSI (*18*). It seems, therefore, likely that the east site is also functionally important in prokaryotes. A study of the flexibility of the *A.v.* PCu molecule, and in particular of the active north site and the potentially active eastern face, is therefore interesting.

MATERIALS AND METHODS

Sample Preparation. Plastocyanin from *A. variabilis* (*A.v.* PCu) was prepared and purified as described previously (*25*). $K^{15}NO_3$ was used as the ^{15}N source in the preparation of the ^{15}N-labeled protein. Aprotinin was added during the purification to minimize the enzymatic degradation of *A.v.* PCu. The 95% ^{15}N-labeled *A.v.* PCu was dissolved in a 90% H_2O/10% D_2O mixture at pH 6.0 (meter reading) to a concentration of 4.1 mM. Unlabeled *A.v.* PCu was dissolved in 99.9% D_2O or a 90% H_2O/10% D_2O mixture at pH 6.9−7.1 (meter reading) at concentrations from 2.8 to 3.2 mM. All samples contained 100 mM NaCl. To maintain the protein in the reduced form, small amounts (0.6−0.7 mM) of sodium ascorbate were added. The solutions were flushed with nitrogen to remove oxygen, and the NMR sample tubes were sealed off under nitrogen.

^{15}N and ^{13}C Assignments. NMR experiments for heteronuclear resonance assignment were recorded on Varian Unity Inova 500 and 750 spectrometers equipped with 5 mm [^1H, ^{15}N, ^{13}C] triple-resonance pulsed-field gradient probes, and a Bruker AM500 spectrometer equipped with an inverse probe and four frequency channels. The ^{15}N assignment was obtained from double-resonance two-dimensional (2D) ^1H−^{15}N HSQC and HSQC-TOCSY spectra (*43*, *44*) and a three-dimensional (3D) TOCSY-HMQC spectrum (*45*, *46*), all recorded on ^{15}N-labeled *A.v.* PCu. Assignment of the backbone $^{13}C^{\alpha}$ resonances was obtained by a combination of a 2D triple-resonance HNCA experiment using a ^{15}N-labeled protein with ^{13}C in natural abundance, and a 2D gradient-enhanced ^1H−^{13}C HSQC (*47*) spectrum. The HNCA spectrum was acquired by using a gradient variant of the HNCA pulse sequence (*50*−*52*) and omitting the evolution period in the ^{15}N dimension. The ^{13}C carrier was placed at the center of the $^{13}C^{\alpha}$ chemical shift region (58.12 ppm). The HNCA experiment correlates the NH protons with the intraresidue $^{13}C^{\alpha}$ nuclei via the $^1J_{NC}{}^{\alpha}$ one-bond coupling (7−12 Hz). Further, it correlates the NH proton with the $^{13}C^{\alpha}$ of the preceding residue via the $^2J_{NC}{}^{\alpha}$ two-bond coupling (<7 Hz). Side chain ^{13}C atoms were assigned using the gradient-enhanced HSQC, HMQC-COSY, and HSQC-TOCSY experiments (*48*, *49*). A mixing time of 40 ms was applied to obtain multiple-bond relayed signals in the HSQC-TOCSY experiment. Backbone carbonyl ^{13}C assignments were obtained by a 2D gradient-enhanced version of the HNCO (*50*−*53*) experiment, using the ^{15}N-labeled sample with ^{13}C in natural abundance. The HNCO spectrum correlates a given NH proton with the carbonyl carbon of the preceding residue via the $^1J_{NC'}$ coupling (∼15 Hz). In the HNCO experiment, the ^{13}C carrier was placed at the center of the carbonyl carbon chemical shift region (176.1 ppm).

^{15}N and ^{13}C Relaxation Measurements. All relaxation experiments were performed at 11.7 T and 298 K. The ^{15}N and ^{13}C longitudinal and transverse relaxation rates R_1 and R_2 and the steady-state [^1H]−^{15}N or [^1H]−^{13}C NOE were measured by HSQC-type experiments (*7*). All the spectra were acquired with hypercomplex quadrature detection using the States−Haberkorn−Ruben method (*54*). The ^{13}C and ^{15}N resonances were decoupled with the WALTZ-16 scheme (*55*) during acquisition. In all the experiments, the ^1H carrier was placed on the HDO residual resonance (4.774 ppm at 298 K). To eliminate errors caused by the systematic drift of the spectrometer, the 2D spectra in each relaxation experiment were recorded simultaneously using a recurrent procedure as described in ref *26*. The relaxation delays in the R_1 and R_2 relaxation series were chosen in a random order.

The ^{15}N relaxation experiments were performed on the ^{15}N-labeled sample with gradient sensitivity-enhanced pulse sequences (*8*). The spectra were collected as 2048 t_2 data points and 320 t_1 slices, and with sweep widths of 10 and 2 kHz in the ^1H and ^{15}N dimensions, respectively. In the R_1 experiment, 11 spectra were recorded with relaxation delays of 0.010, 0.020, 0.040, 0.080, 0.160, 0.321, 0.501, 0.702, 0.903, 1.203, and 1.905 s, respectively. In the R_2 experiment, 10 spectra were recorded with relaxation delays of 0, 17, 33, 50, 67, 83, 100, 116, 150, and 183 ms, respectively. The relaxation delay was implemented as a train of CPMG sequences (*56*) with a delay of 0.9 ms between subsequent ^{15}N 180° pulses and with dipole−dipole/CSA cross-correlation suppression implemented as in Figure 10b of ref *8*. A recovery delay of 1.5 s was applied between scans, and eight scans were recorded for each slice in the R_1 and R_2 relaxation series. The entire data collection time was 19.5 and 12.5 h for the R_1 and R_2 series, respectively. The steady-state [^1H]−^{15}N NOEs were estimated from ^{15}N-excited HSQC spectra recorded with and without ^1H presaturation. A train of 120° ^1H pulses separated by 5 ms delays was applied to obtain the ^1H presaturation (*57*). In the spectra recorded without the ^1H presaturation, the recovery delay was 4 s. In the spectra recorded with the ^1H presaturation, the recovery delay consisted of a 1 s delay followed by presaturation for 3 s. Two identical pairs of spectra with and without presaturation were recorded simultaneously, and the average of the corresponding signals in the two pairs was used in the estimation of the NOEs.

The ^{13}C relaxation measurements included only the methine carbons. The measurements were performed on samples with ^{13}C in natural abundance, using the 2D heteronuclear ^1H−^{13}C experiment by Palmer et al. (*16*) and modified by Mispelter et al. (*17*). All spectra were acquired with 2048 t_2 data points and 256 t_1 slices and sweep widths of 6025 and 4400 Hz in the ^1H and ^{13}C dimensions, respectively. The ^{13}C R_1 rates were measured as described previously (*26*). Nine spectra were recorded in the R_1 series with relaxation delays of 0.01, 0.1, 0.2, 0.4, 0.8, 1.2, 1.8, 2.5, and 4.5 s, respectively. In the R_2 experiment, a CPMG spin-echo period of 0.5 ms was used. The recovery delay between scans was 1.7 s, while 192 scans were performed for each slice. Eleven spectra were acquired with relaxation delays of 1, 5, 10, 15, 20, 25, 30, 40, 50, 60, and 70 ms, respectively. The entire acquisition times were 13.5 and 12.3 days for the R_1 and R_2 experiments, respectively. In the steady-state [^1H]−^{13}C NOE experiment, two spectra were obtained, one with ^1H presaturation and one without. The latter spectrum was recorded with a recovery delay of 4.4 s, while the former was recorded with a 4.4 s train of short 90° ^1H pulses separated by delays of 7 ms to obtain the ^1H presaturation. The entire acquisition time was 7 days.

The relaxation spectra were processed with the program NMRPipe (*58*). The FIDs were zero-filled to 4096 and 1024 data points in the t_2 and t_1 dimensions, respectively, in the ^{15}N experiments and to 4096 and 512 data points, respectively, in the two dimensions in the ^{13}C experiments. An exponential line broadening of 5 Hz was applied in the t_2

dimension, while a sine-bell window function was applied in the t_1 dimension. No baseline correction was used.

Relaxation Data Analysis. The intensities of the signals in the relaxation spectra were measured by the volumes of the cross-peaks in the 2D $^1H-^{15}N$ or $^1H-^{13}C$ spectra, using a total least-squares (LSQ) fitting procedure (*59*, *60*). The R_1 and R_2 relaxation rates of the ^{15}N nuclei were estimated by a LSQ fit of a two-parameter exponential decay function to the signal intensities (*7*, *16*), while the R_1 and R_2 relaxation rates of the ^{13}C nuclei were estimated by a LSQ fit of three-parameter and two-parameter exponential functions, respectively (*17*). The steady-state heteronuclear NOEs were calculated with the relation NOE $= I_{sat}/I_{unsat}$, where I_{sat} and I_{unsat} are signal intensities corresponding to spectra with and without ^1H saturation, respectively. In the ^{15}N case, the NOEs of a given signal were calculated from the average of the intensities in the two identical spectra. The uncertainties of the signal intensities were estimated from the root-mean-square noise level in the spectra. The uncertainties of the R_1 and R_2 rates were estimated by Monte Carlo simulation. The uncertainties of the steady-state heteronuclear NOEs were calculated by error propagation.

Rotational Diffusion Anisotropy. The overall rotation of the molecule was analyzed to separate its contributions to relaxation from those of site-specific internal motions. The protocol used for the analysis of the relaxation data is based on the procedure reported previously (*5*, *61*). Residue-specific correlation times were derived from the R_2/R_1 ratios (*7*). Subsequently, an overall, isotropic correlation time for the protein was calculated from their 15% trimmed average, together with the corresponding maximal NOE (*62*). An estimation of the components of the molecular rotational diffusion tensor was made using the coordinates of the energy-minimized average structure of *A.v.* PCu [PDB entry 1FA4 (*26*)]. The rotational diffusion tensor was assumed to be axially symmetric. Subsequently, the overall correlation time [$\tau_m = (2D_{||} + 4D_\perp)^{-1}$], the rotational diffusion anisotropy ($\eta = D_{||}/D_\perp$), and the direction of the principal component of the rotational diffusion tensor in the molecular frame, as defined by two spherical coordinates θ and ϕ, were estimated simultaneously by fitting the experimental R_2/R_1 ratios to values calculated for an axially symmetric diffusor (*63*, *64*). Residues with NOEs that are less than 75% of the maximal NOE and residues with unknown NOEs were excluded from the calculation to avoid interference from residues affected by substantial internal dynamics. Furthermore, residues for which

$$\frac{\langle R_2^{-1}\rangle - R_2^{-1}}{\langle R_2^{-1}\rangle} - \frac{\langle R_1^{-1}\rangle - R_1^{-1}}{\langle R_1^{-1}\rangle} > 1.5 \times \mathrm{SD} \qquad (1)$$

where SD is the standard deviation of the values of the left side for all residues considered were not included in the analysis due to possible conformational exchange contributions to R_2 (*64*). *F* statistics testing was used to evaluate the significance of the axially symmetric model as compared to the isotropic model (*15*).

Model-Free Analysis. The relaxation data were analyzed according to the extended Lipari−Szabo model-free formalism (*65*−*67*), using the model-free spectral density function of the NH bond vector or the methine CH bond vector as described by Palmer et al. (*61*)

$$J(\omega) = \frac{2}{5}\left[\frac{S^2\tau_m}{1+(\omega\tau_m)^2} + \frac{(1-S_f^2)\tau_f'}{1+(\omega\tau_f')^2} + \frac{(S_f^2-S^2)\tau_s'}{1+(\omega\tau_s')^2}\right] \qquad (2)$$

where $\tau_f' = \tau_f\tau_m/(\tau_f + \tau_m)$, $\tau_s' = \tau_s\tau_m/(\tau_s + \tau_m)$, τ_m is the overall rotational correlation time of the molecule, τ_f is the effective correlation time for internal motions (τ_i) on a fast time scale defined by $\tau_f < 100-200$ ps, and τ_s is the effective correlation time for internal motions (τ_i) on a slow time scale defined by $\tau_f < \tau_s < \tau_m$. Further, S^2 ($=S_f^2S_s^2$) is the square of the generalized order parameter characterizing the amplitude of the internal motions, and S_f^2 and S_s^2 are the squares of order parameters for the internal motions on the fast and slow time scales, respectively. Order parameters quantify the amplitudes of the motions of the NH or $C^\alpha-H^\alpha$ bond vectors on the picosecond to nanosecond time scale, with values ranging from 0 for isotropic internal motions to 1 for completely restricted motion in a molecular frame. In addition to the fast picosecond to nanosecond motion, slow dynamics on the microsecond to millisecond time scale affect the R_2 rates, leading to an exchange contribution, R_{ex}. This contribution is caused by the fluctuation of the chemical shift on the microsecond to millisecond time scale. The magnitude of the R_{ex} contribution is governed by the exchange rates, the chemical shift difference and the relative populations of the different states, and the refocusing delay in the CPMG pulse sequence applied in the R_2 experiment.

Model-free parameters were calculated on a per residue basis by a grid search followed by a nonlinear LSQ minimization procedure while keeping the overall rotational diffusion parameters constant. The uncertainties of the model-free parameters were estimated using Metropolis−Monte Carlo simulations with 500 randomly distributed synthetic data sets. In analogy to the model selection method introduced by Mandel et al. (*61*, *68*), one of five models was selected for each site. The procedure uses Monte Carlo simulations combined with χ^2 and *F* statistics testing for selecting the most appropriate model. Critical α values of 0.05 and 0.2 were used in the χ^2 and *F* statistics testing, respectively. The regression parameters of the five models are as follows: model 1, S^2 only by assuming $S_s^2 = 1$ and $\tau_f \rightarrow 0$; model 2, S^2 and τ_i assuming $S_s^2 = 1$; model 3, S^2 and R_{ex} assuming $S_s^2 = 1$ and $\tau_f \rightarrow 0$; model 4, S^2, τ_i, and R_{ex} assuming $S_s^2 = 1$; and model 5, S^2, S_f^2, and $\tau_i = \tau_s$ by assuming $\tau_f \rightarrow 0$. Models 3 and 4 allow an exchange contribution R_{ex} to transverse relaxation. Model 5 coincides with model 2 in the limit $S_s^2 \rightarrow 1$. Sites for which none of the five models passed the χ^2 test were parametrized with the model selected by exclusively using *F* statistics testing.

RESULTS

^{15}N and ^{13}C Assignments. All ^{15}N resonances observed in the $^1H-^{15}N$ HSQC spectrum were assigned. This includes 95 backbone amide ^{15}N (105 − 9 prolines and the N-terminal Glu1) and eight side chain ^{15}N atoms [N^ϵ of His39(37) and Arg93(88), N^δ atoms of the four asparagine residues, and N^ϵ atoms of the two glutamine residues]. The assigned ^{13}C resonances include all C^α and C^β atoms, 98% of the remaining proton-bearing side chain ^{13}C atoms, and ∼80% of the carbonyl carbons. Twelve of the carbonyl carbons

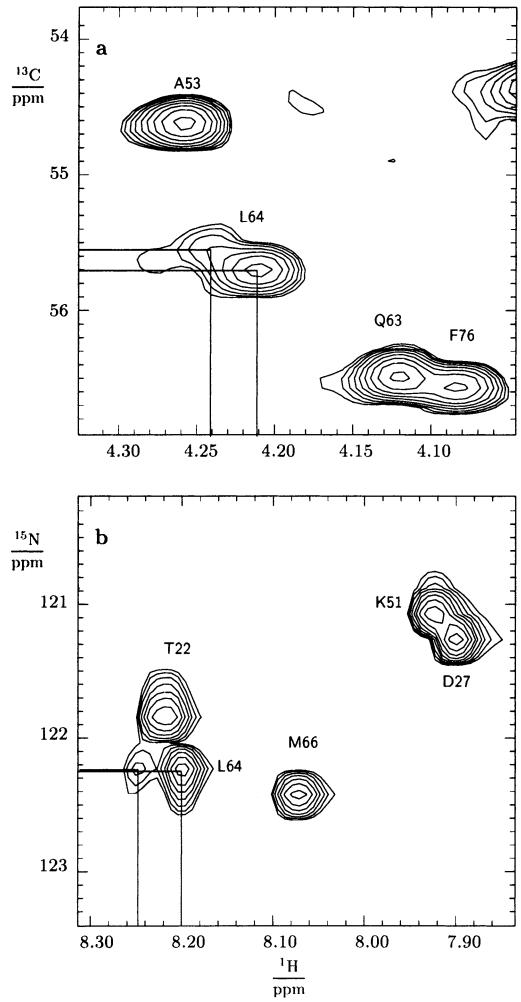

FIGURE 2: Observed double signals of Leu64(62) in the (a) ^{1}H−^{13}C HSQC spectrum recorded on a 2.86 mM *A.v.* PCu sample at 298 K at a magnetic field strength of 17.6 T and (b) ^{1}H−^{15}N HSQC spectrum recorded on the 95% ^{15}N-labeled *A.v.* PCu sample (4.1 mM, 298 K) at a magnetic field strength of 11.7 T.

could not be assigned in the HNCO spectra mainly due to the ambiguities of some of the NH proton chemical shifts, while the carbonyl carbons of the C-terminal residue and the nine carbonyl carbons of the residues preceding the prolines were not observed. Thus, a total of 83 carbonyl carbons were assigned. The chemical shift indices (*69*) of the assigned $^{13}C^{\alpha}$ and $^{13}C'$ nuclei are in good agreement with the secondary structure of the backbone of *A.v.* PCu (*26*, *70*), although the strand β_5 of the structure (Figure 1) was not indicated by the ^{13}C or the ^{1}H chemical shift indices (see below).

In addition to the ^{15}N and ^{13}C assignments, the previous ^{1}H assignments (*25*) were largely confirmed and further extended. Some of the previously ambiguous assignments were clarified using the NMR spectra of partially oxidized *A.v.* PCu (*26*). Thus, the protons of Glu90(85), Pro91(86), His92(87), Arg93(88), and Met97(92) could be identified unambiguously from the signal broadening in the partly oxidized samples caused by the nearby paramagnetic copper ion.

Two sets of resonances were observed for Leu64(62) in the ^{1}H−^{13}C HSQC, ^{1}H−^{15}N HSQC (Figure 2), HNCA, and NOESY spectra. This shows that Leu64(62) exists in two conformations. Also, Pro38(36) shows double signals in the ^{1}H−^{13}C HSQC spectrum, indicating a cis−trans isomerization around the Pro37(35)−Pro38(36) peptide bond (*71*). Two of the aromatic ring carbons, C^{δ} and C^{ϵ} of Tyr85(80), were not observed in any of the ^{1}H−^{13}C correlated spectra, indicating high mobility for the aromatic ring of Tyr85(80). A complete list of the ^{15}N, ^{13}C, and ^{1}H assignments is given in Supporting Information and has been deposited in the BioMagResBank under accession number 5505.

Relaxation Parameters. R_1 and R_2 relaxation rates and NOE data were obtained for 89 of the 95 assigned backbone ^{15}N nuclei. In addition, relaxation data were obtained for N^{ϵ} of His39(37) and N^{ϵ} of Arg93(88). The experimental ^{15}N data resulted in relaxation parameters with low standard deviations (Figure 3), allowing small R_{ex} exchange contributions to be estimated (Figure 5). None of the NOE values exceeds the theoretical maximum of 0.78 with more than one standard deviation. A determination of the relaxation parameters of the remaining six NH groups was obscured by overlapping signals [Thr2(0)/Ser9(7), Ala19(17)/Lys35-(33), and Val36(34)/Tyr88(83)]. The R_1 and R_2 rates, the R_2/R_1 ratios, and the NOE values obtained for the backbone ^{15}N nuclei are shown in Figure 3. The 15% trimmed mean values of R_1, R_2, and R_2/R_1 are 2.14 ± 0.01 s^{-1}, 8.00 ± 0.05 s^{-1}, and 3.74 ± 0.02, respectively. The average of the NOE values of all residues except Gly105(100) is 0.75 ± 0.02. The NOE value of Gly105(100) is negative (−0.595 ± 0.006), and its R_1 and R_2 rates are significantly lower than the average rates. These results indicate large-amplitude internal motions on the fast time scale (picoseconds to nanoseconds) of the C-terminal end of the protein. In the Lys10(8)−Leu13(11), Ala45(43)−Leu47(45), Ala53(51)−Lys57(55), Lys62(60)−Gln63(61), Ser73(71), Ala82(77), Thr86(81), His92(87)−Gly94(89), and Met97(92)−Gly99-(94) regions, the R_2 values and R_2/R_1 ratios are elevated significantly above the average values. These results indicate slow conformational rearrangements on the microsecond to millisecond time scale in five of the loops of *A.v.* PCu, and in the α-helix and strands β_6 and β_7.

The ^{13}C relaxation data (at 11.7 T and 298 K) are less precise due to the use of ^{13}C in natural abundance and relatively low protein concentrations, and in some cases severe signal overlap. Still, complete sets of R_1, R_2, and NOE values were obtained for 77 of the $^{13}C^{\alpha}$ atoms of *A.v.* PCu (Figure 4). The 15% trimmed mean values of R_1, R_2, and R_2/R_1 are 1.68 ± 0.11 s^{-1}, 24.8 ± 1.7 s^{-1}, and 14.8 ± 0.2, respectively. The ^{15}N and ^{13}C relaxation data of *A.v.* PCu are given in the Supporting Information and have been deposited in the BioMagResBank under accession number 5505.

Rotational Diffusion Tensor and Overall Correlation Time. The rotational diffusion property of *A.v.* PCu was estimated as described in Materials and Methods. The overall correlation time τ_m was based on a total of 63 and 53 residues, respectively, using the ^{15}N relaxation and ^{13}C relaxation data. The estimated correlation times were 6.26 ± 0.02 and 6.10 ± 0.05 ns, respectively, assuming an isotropic rotational diffusion. The small difference between the τ_m values obtained from the ^{15}N and ^{13}C data could be due to the difference in the protein concentrations and D_2O concentrations used in the two samples.

The normalized lengths of the principal axes of the inertia tensor for *A.v.* PCu were calculated from the energy-

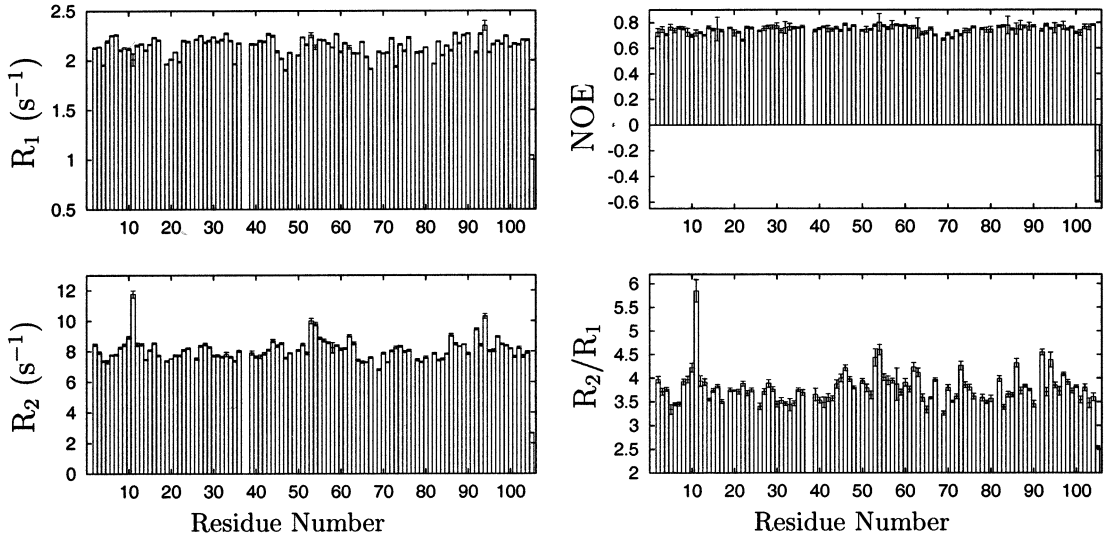

FIGURE 3: Plots of the experimental ^{15}N R_1 and R_2 relaxation rates, the steady-state [^{1}H]−^{15}N NOE data, and the R_2/R_1 ratios for *A.v.* PCu at 298 K and a magnetic field strength of 11.7 T.

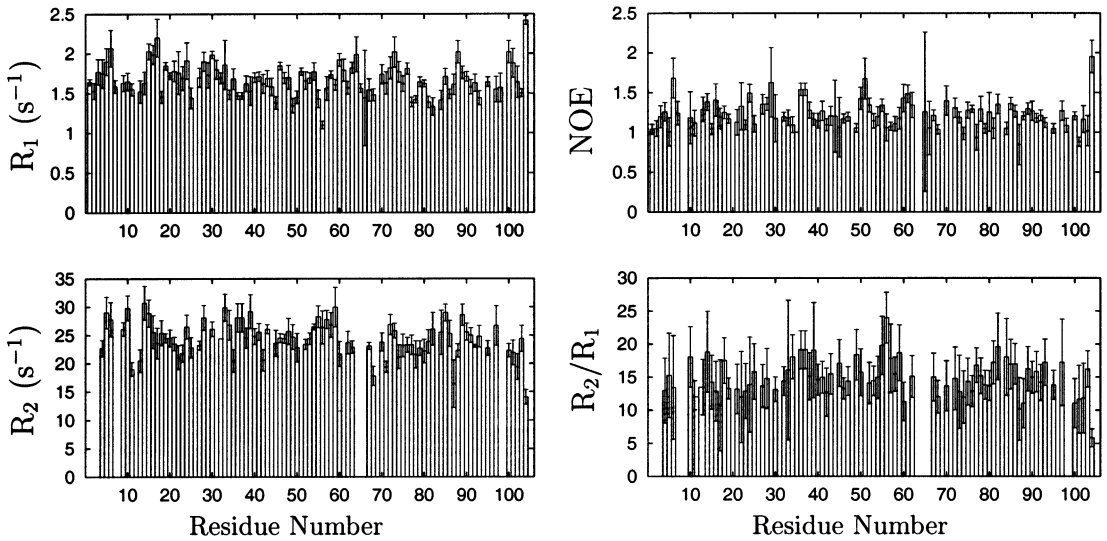

FIGURE 4: Plots of the experimental ^{13}C R_1 and R_2 relaxation rates, the steady-state [^{1}H]−^{13}C NOE data, and the R_2/R_1 ratios for *A.v.* PCu at 298 K and a magnetic field strength of 11.7 T.

minimized average structure [PDB entry 1FA4 (*26*)], yielding a ratio of 1.00:0.67:0.60. Since the PCu molecule is prolate, the ^{15}N data also were analyzed using the axial symmetric rotational diffusion tensor model. Residues with substantial internal dynamics (NOE that is less than 75% of the maximal NOE) were excluded from the analysis as outlined in Materials and Methods. These residues are the C-terminal Gly105(100) and residues with substantial exchange contributions to R_2 (eq 1), i.e., Lys11(9), Ala53(51), Asp54(52), Ser73(71), Thr86(81), His92(87), and Gly94(89). The F statistics test indicates that the ^{15}N relaxation data were better described by the axially symmetric rotational diffusion model than by the corresponding isotropic model ($F = 6.87$). The values of the correlation time τ_m, the ratio $D_{||}/D_{\perp}$, and the spherical coordinates θ and ϕ obtained using the axially symmetric model were therefore used to analyze the internal dynamics from the ^{15}N relaxation data of *A.v.* PCu. The optimized effective τ_m was 6.23 ns, and the rotational diffusion anisotropy was $D_{||}/D_{\perp} = 1.15$.

Model-Free Analysis. The experimental relaxation parameters of each residue were analyzed with each of the five models described in Materials and Methods, using the spectral density function in eq 2. The model-free approach and the axially symmetric diffusion model were used in the analysis of ^{15}N relaxation data. However, the obtained model-free parameters did not deviate beyond the uncertainty of those obtained using the isotropic model. The S^2, R_{ex}, and τ_i parameters were obtained for 79 backbone nitrogens and two side-chain nitrogens, His39 N$^{\epsilon}$ and Arg93 N$^{\epsilon}$, according to the χ^2 test criterion for the five models. For nine of the residues, the simplest model 1 could account for the relaxation data. For nine of the nitrogens, the relaxation data could be described by model 2 that includes a fast internal motion (τ_i) τ_f (∼20−200 ps), while 19 nitrogens agreed with model 3 where a small R_{ex} term accounts for conformational rearrangements on the microsecond to millisecond time scale. The relaxation data of 26 nitrogens were described by model 4 that requires both an internal motion (τ_i) τ_f and a small R_{ex} exchange term to account for the dynamics of the protein. The substantial number of sites fitted with model 4 is a consequence of the high signal-to-noise ratio of the relaxation data. When alternatively fitted to models 2 and 3, eight and

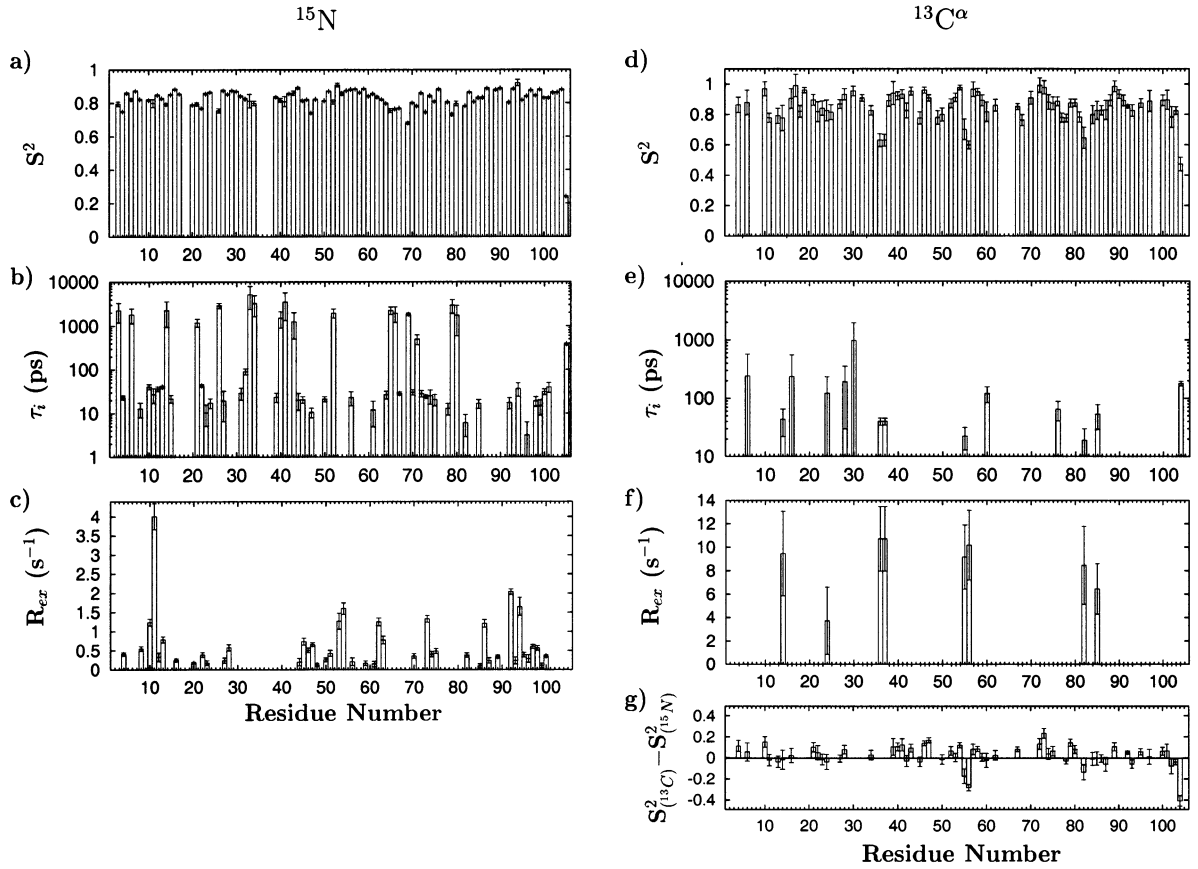

FIGURE 5: Results from the model-free analysis of the ^{15}N (a−c) and $^{13}C^{\alpha}$ (d−f) relaxation data as a function of the protein sequence of *A.v.* PCu: (a and d) order parameters S^2, (b and e) internal correlation times τ_i, and (c and f) exchange terms R_{ex}. The differences between the ^{15}N and $^{13}C^{\alpha}$ order parameters are shown in panel g.

nine sites could be fitted to the models, respectively, with a χ^2 of <10. The estimated model-free parameters do not change notably when fitted with model 2 or 3. Further, the relaxation data of 18 nitrogens could be fitted only by model 5 that involves internal motion on two time scales, both faster than the overall molecular diffusion. Finally, 11 nitrogens, which failed the χ^2 test for all five models, were evaluated according to the *F* statistics selection criterion, exclusively. Thus, models 1−3 were fitted to the relaxation parameters of eight nitrogens, one nitrogen, and one nitrogen, respectively. The model-free parameters that were obtained are shown in Figure 5a−c.

The generalized order parameters S^2 are in the range of 0.68−0.92 for ^{15}N, except for the C-terminal Gly105(100) ($S^2 = 0.24$). The average order parameter is 0.83 ± 0.05. R_{ex} exchange contributions ranging from 0.10 to 4.01 s^{-1} were observed for 45 backbone amide atoms. An internal correlation time was determined for 55 amide nitrogen atoms The effective correlation times for 37 nitrogens ranged from 3.2 to 91.1 ps, showing the presence of internal motions on the fast time scale. Eighteen nitrogens showed internal motion on two time scales, with effective correlation times of the slow internal motions in the range of 0.38−5.17 ns. Additionally, the relaxation parameters of N$^{\epsilon}$ of His39(37) and Arg93(88) were analyzed using the isotropic model. The data from N$^{\epsilon}$ of His39(37) were fitted to model 3, where $S^2 = 0.81 \pm 0.01$ and $R_{ex} = 4.4 \pm 1.1$ s^{-1}. Correspondingly, the Arg93(88) N$^{\epsilon}$ data were fitted to model 4 where $S^2 = 0.42 \pm 0.01$, $\tau_i = 58 \pm 3$ ps, and $R_{ex} = 2.8 \pm 0.5$ s^{-1}.

The ^{13}C relaxation data (Figure 5d−f) were too inaccurate to incorporate rotational anisotropy in the model-free analysis. A total of 59 of the 77 C^{α} atoms, for which a complete set of R_1, R_2, and NOE values had been obtained, were fitted to model 1. Because of the relatively large uncertainties of the ^{13}C relaxation parameters, most of the carbons were modeled satisfactorily with model 1, allowing only the order parameters to be obtained. In addition, seven carbons were fitted to model 2 and one was fitted to model 3, while another seven carbons were fitted to model 4. None of the carbons were fitted to model 5.

DISCUSSION

Overall Flexibility of A.v. PCu. In general, the model-free parameters show that the structure of *A.v.* PCu is rigid, as found for other blue copper proteins (*72*), including PCu from the cyanobacterium *Synechocystis* (*73*). Thus, except for the C-terminus, the order parameters of the amide ^{15}N of *A.v.* PCu deviate by less than 0.2 from an average of 0.83, as normally found for proteins with a well-defined secondary structure. Similarly, the order parameters of the $^{13}C^{\alpha}$ atom deviate by less than 0.3 from an average value of 0.86. Also, only a slight increased flexibility on the picosecond to nanosecond time scale is observed in some regions, mainly in loops and regions outside the β-sheet structure. However, moderate yet significant exchange contributions are observed for a series of residues, indicating mobility on the microsecond to millisecond time scale. Moreover, most of these residues cluster in certain regions, mainly on the north site

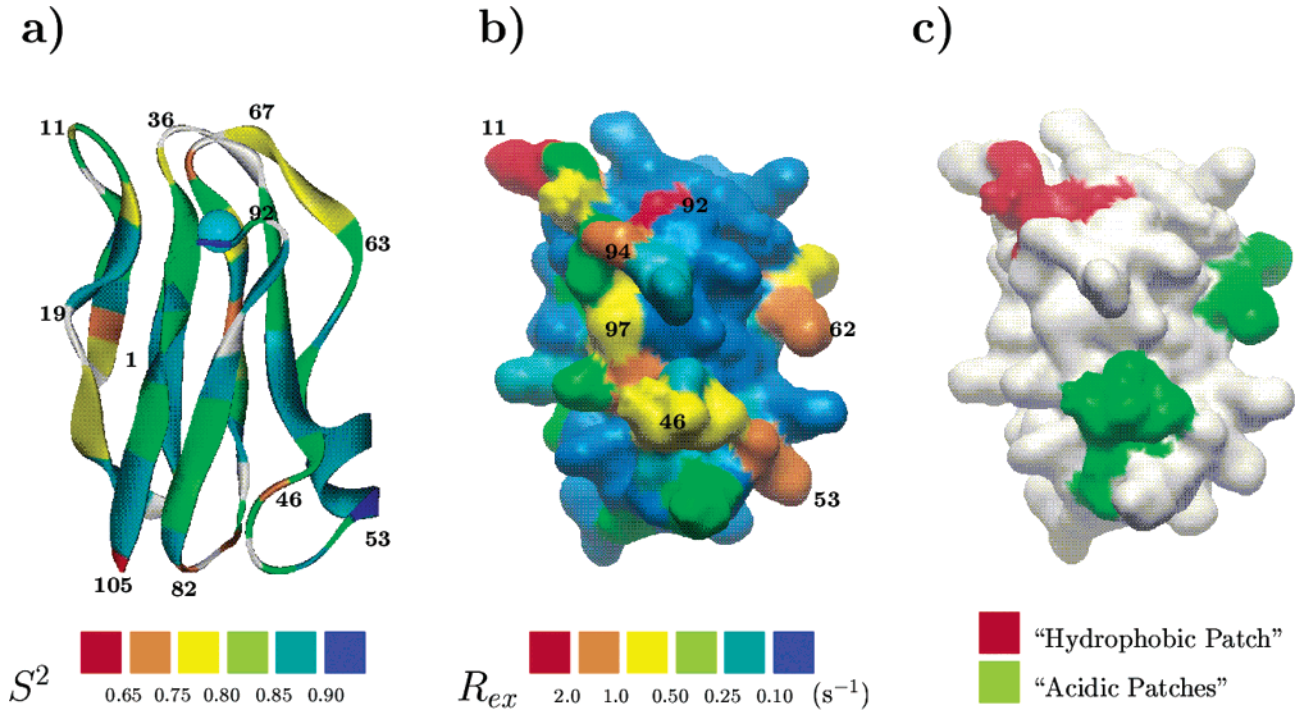

FIGURE 6: Solution structure of *A.v.* PCu (PDB entry 1FA4) showing regions with enhanced motion of the amide ^{15}N nuclei (a) on the picosecond to nanosecond time scale (S^2) and (b) on the microsecond to millisecond time scale (R_{ex}). In panel c are shown the regions important in eukaryotic organisms for the complex formation with Cyt *f* and/or PSI (*28*). These regions correspond largely to the regions shown in panel b that exhibit microsecond to millisecond motion.

and the eastern face of *A.v.* PCu (Figure 6). Most interestingly, these regions not only correspond to the regions that are involved in the electron-transfer processes of eukaryotic plastocyanins (*28*−*30*) but also are important for the activity of prokaryotic plastocyanins (*39*−*41*), as discussed below.

Mobility of the North Site of A.v. PCu. The mobility of the $\beta_7-\beta_8$ loop is of special interest. This loop contains three of the copper ligands, Cys89(84), His92(87), and Met97(92) (in the following called the Cys-His-Met loop). The amide ^{15}N nuclei of residues Cys89(84), His92(87), Gly94(89), Ala95(90), Gly96(91), Met97(92), and Val98(93) all have R_{ex} contributions (Figures 5c and 6b). In particular, it is interesting that copper ligands His92(87), Met97(92), and Cys89(84) are affected by microsecond to millisecond dynamics, indicating structural fluctuations of the Cys-Met-His loop. Also, the copper binding imidazole ring of His39(37) has increased mobility on this time scale, as shown by the R_{ex} contribution ($R_{ex} = 4.4 \pm 1.1$ s^{-1}) to the relaxation of the $^{15}N^{\epsilon}$ atom. Thus, the entire copper site shows microsecond to millisecond dynamics. A similar mobility of residues close to the copper ion was observed in PCu from the cyanobacterium *Synechocystis* (*73*). The copper site fluctuation could be caused by a protonation and/or deprotonation of the imidazole ring of His92(87). Thus, the imidazole ring has a pK_a value of 5.1 (*37*, *74*), while the experiments here were performed at pH 6. Therefore, the protonated form is significantly populated, and this may result in the observed R_{ex} contributions, depending on the exchange rate between the protonated and deprotonated forms. However, the exchange may also reflect a fluctuation of the Cys-His-Met loop independent of the protonation of His92(87).

No significant mobility of the Cys-His-Met loop on the faster picosecond to nanosecond time scale was indicated by the relaxation data. Only His92(87) has order parameters that are slightly lower than the average values (0.80 for the amide ^{15}N atom and 0.85 for the $^{13}C^{\alpha}$ atom), while most of the other residues in the Cys-His-Met loop have higher than average order parameters. The unusually high side chain order parameter (0.81) of the imidazole $^{15}N^{\epsilon}$ of His39(37) is in accordance with the binding of the imidazole ring to the copper ion and with the strong hydrogen bonding observed for the NH^{ϵ} group.

Overall, the results show that the Cys-His-Met loop is flexible on the microsecond to millisecond time scale but rigid on the picosecond to nanosecond time scale. Since most biological reactions, including the electron-transfer reaction, take place on the microsecond to millisecond time scale, the flexibility observed here might be necessary for the copper site to adapt its structure to the most favorable conformation for electron transfer upon complex formation, and to ensure a low reorganization energy when going from the reduced to the oxidized form. Previously, Malmström (*75*) and Sigfridsson (*19*) have discussed the dependence of the electron-transfer properties on the mobility of the copper ligands. It should also be noted that the sequence of Gly94(89), Ala95(90), and Gly96(91) in the Cys-His-Met loop is preserved in all plastocyanins [except one (*76*)] and that the glycines with their high degree of conformational freedom might be necessary to ensure the flexibility. Furthermore, the guanidyl group of Arg93(88) displays dynamics on both fast and slow time scales, indicating that there is both a significant exchange contribution and a low order parameter. Also, this residue is highly preserved, and it has been suggested (*77*) that it is important for the function of prokaryotic plastocyanins. Finally, it has been suggested (*22*) that the $\pi-\pi$ interactions between Tyr88(83) and the guanidyl group of Arg93(88), observed in the X-ray structure

of prokaryotic PCu from *Synechococcus*, moves the Cys-His-Met loop slightly away from the copper center, and that this interaction might be crucial for the regulation of the mobility and structure of the Cys-His-Met loop and thereby the geometry of the copper site (*78*).

The $\beta_3-\beta_4$ loop, which is part of the hydrophobic surface of the north site and includes the copper ligand His39(37), also has enhanced mobility as indicated by the R_{ex} contributions and low order parameters of the $^{13}C^{\alpha}$ nuclei of Val36-(34) and Pro37(35). Although the interpretation of these data is less certain because of the overlap of the two signals, at least one of the residues exhibits increased mobility. The double signals that are observed for the $^{13}C^{\gamma}$ atom of Pro38-(36) were ascribed to cis−trans isomerization of the Pro37-(35)−Pro38(36) bond (*71*) and are also in accordance with increased mobility in this region. Thus, both the microsecond to millisecond mobility of the $\beta_3-\beta_4$ loop and the presence of two local conformations in the loop could be functionally relevant.

Mobility of the Eastern Face of A.v. PCu. Moderate R_{ex} exchange contributions are observed in the $\beta_4-\alpha$ [Asp44-(42)−Lys51(49)] and $\alpha-\beta_5$ [His61(59)−Gln63(61)] loop regions. These regions correspond to the large and small acidic patches, respectively, in eukaryotic plastocyanins (Figure 6b,c). The R_{ex} exchange of the $\alpha-\beta_5$ loop could be caused by protonation and/or deprotonation of the imidazole of His61(59), possibly linked to the reorientation of the imidazole ring, similar to that observed for azurin (*79*). Thus, the loop clusters around the side chain of His61(59), together with residues Ser73(71)−Thr75(73) that also have R_{ex} exchange contributions, while the imidazole of His61(59) has a pK_a of 7.3 (*74*).

The smaller order parameters observed in the short strand β_5 [Gln63(61)−Ser67(65)] adjacent to the $\alpha-\beta_5$ loop (Figure 6a) are also of interest. According to the structure calculation (*26*), the structure of the strand is relatively loose. This is confirmed by the chemical shifts since neither the $^{1}H^{\alpha}$ (*25*) nor the $^{13}C^{\alpha}$ and $^{13}C'$ chemical shift indices (*70*) indicate a β-sheet in this region. In addition, strand β_5 contains several hydrophobic residues. Strand β_5 could, therefore, be a part of the hydrophobic interaction surface. The loose and flexible structure of the strand is further suggested by the double signals of Leu64(62) (Figure 2) corresponding to two local conformations in this region, and by the "slow" motion on the picosecond to nanosecond time scale with similar correlation times ($\tau_s \approx 2$ ns) of Leu65(63), Met66(64), and Gly69(67), which indicate a concerted motion of these residues on the fast time scale. Hence, the eastern face of *A.v.* PCu, including the region that corresponds to the acidic patch of eukaryotic plastocyanins, is flexible on a variety of time scales from picoseconds to seconds, as expected for regions involved in the interaction with the reaction partners Cyt *f* and PSI.

The functional importance of the eastern face in prokaryotes is not fully clarified. Recent site-directed mutagenesis and kinetic studies of plastocyanin and cytochrome *f* (Cyt *f*) of cyanobacterium *P. laminosum* (*40*) indicate that the eastern face is involved in the complex formation with Cyt *f*, although not to the same extent as in eukaryotes. Thus, it was suggested that transient conformations of the complex of PCu and Cyt *f* involving the east site increase the number of productive collisions. However, Crowley et al. (*39*) were unable to detect any direct interaction of the eastern face of *P. laminosum* plastocyanin with Cyt *f* through intermolecular pseudo-contact shifts of plastocyanin nuclei in the presence of oxidized (paramagnetic) Cyt *f*. Still, the complex may be too short-lived and transient to be visible using this approach. Indeed, by using an NMR approach that exploits the more sensitive intermolecular nuclear paramagnetic relaxation enhancement, it was shown recently (*41*) that not only the north site but also the eastern face of *A.v.* PCu participates in the formation of short-lived, transient intermolecular interactions. This correlates well with the dynamics results obtained here, and with the general observation that protein binding sites are often flexible and can be seen as "soft" spots on the protein surface that easily can adapt to a binding partner.

Other Mobile Regions of A.v. PCu. The highly solvent-exposed $\beta_1-\beta_{2A}$ loop [residues Gly8(6)−Leu13(11)] displays microsecond to millisecond motion. Here Leu13(11), as part of the hydrophobic patch, may be important in complex formation. Also, the first part of the α-helix [Ala53(51)−Ser60(58)] has mobility on the microsecond to millisecond time scale according to both the ^{15}N and ^{13}C data, in agreement with the relatively flexible structure of the helix.

Finally, the region of Tyr85(80) and Thr86(81) in strand β_7 was found to be flexible as evidenced by R_{ex} exchange contributions. This could be caused by a reorientation of the aromatic ring of Tyr85(80). The aromatic signals of Tyr85-(80) were absent in the $^{1}H-^{13}C$ correlated spectra, which suggest mobility of also the aromatic ring. Ala82(77) in the southern $\beta_6-\beta_7$ loop also has R_{ex} contributions according to both the ^{15}N and ^{13}C data.

Significance of the $^{13}C^{\alpha}$ Relaxation Data. The $^{13}C^{\alpha}$ relaxation data provide additional information about the dynamics of PCu compared to the normally used ^{15}N data. In particular, the $^{13}C^{\alpha}$ data are valuable in the case of prolines and other residues where the ^{15}N relaxation parameters cannot be obtained.

For most residues here, the sequential variations of the ^{15}N and $^{13}C^{\alpha}$ order parameters follow the same trend, although the uncertainty of the $^{13}C^{\alpha}$ data is considerably larger than that of the ^{15}N data, since natural abundance ^{13}C was used. However, in some regions, the order parameters of the $^{13}C^{\alpha}$ atoms deviate significantly from those of the adjacent amide ^{15}N nuclei (Figure 5g). This holds in particular for Ala104(99), which has a rather low C^{α} order parameter ($S_f^2 = 0.47$) similar to that of the neighboring amide ^{15}N of the C-terminal Gly105(100) ($S_f^2 = 0.43$). In contrast, the amide ^{15}N order parameter of Ala104(99) is high ($S_f^2 = 0.88$), in agreement with the hydrogen bond formed by this amide group as part of the strand β_8. The low order parameter of the C^{α} atom of Ala104(99) is a clear indication of a high flexibility of the $N-C^{\alpha}$ bond of Ala104(99). Similar $^{13}C^{\alpha}$ order parameters that are significantly lower than the order parameters of the amide ^{15}N nuclei of the same residue are found for Leu55(53) and Ala56(54). These residues are located in the α-helix of *A.v.* PCu [Ala53(51)−Ser60(58)] which is a relatively flexible helix, as indicated by the observed R_{ex} exchange contributions, the fast NH exchange of Ser58(56) (*25*), and the relatively few medium-range NOEs (*25*, *26*, *70*). Still, this can hardly explain the observed discrepancy between the ^{15}N and C^{α} order parameters.

It should be noted that the R_{ex} contributions obtained for adjacent ^{15}N and $^{13}C^{\alpha}$ nuclei cannot be compared directly, unless in the slow exchange limit (*80*). Above that limit, the R_{ex} rates depend on the variations in the chemical shift of the nuclei experienced during the motion. These variations can be very different for $^{13}C^{\alpha}$ and amide ^{15}N.

Concluding Remarks. This study shows that plastocyanin from the cyanobacterium *A. variabilis* is a highly rigid protein. Yet, there are regions with slightly enhanced picosecond to nanosecond backbone flexibility, and regions with moderate microsecond to millisecond dynamics. The regions undergoing microsecond to millisecond motion largely coincide with regions which are important for the function of plastocyanin. These regions are, primarily, the copper site and the hydrophobic region on the north side. The mobility of the residues close to the copper center is of particular interest since it reflects multiple conformations of this site. However, the microsecond to millisecond mobility of the eastern face of the *A.v.* PCu molecule, corresponding to the acidic patches of eukaryotic PCu, is also interesting in light of recent findings (*40*, *41*) that this region is also important for the function of prokaryotic plastocyanins, including their complex formation with Cyt *f*.

Finally, the study confirms that relaxation measurements of ^{13}C in natural abundance are feasible and can be used to obtain information of acceptable accuracy about the dynamics in proteins. Also, the derived order parameters are in reasonable agreement with those obtained from ^{15}N relaxation measurements. In particular, the ^{13}C data here provide proline dynamics information that cannot be obtained from the ^{15}N data. As demonstrated previously, ^{13}C relaxation studies hold great promise for studies of side chain mobility (*81*, *82*). In this study, the total acquisition time for the ^{13}C experiments was quite extensive. However, at a higher field strength and with more sensitive probes (such as cryoprobes), the acquisition time can be lowered and the accuracy can be increased drastically.

ACKNOWLEDGMENT

We are grateful to Mrs. Else Philipp and Dr. Jens Duus for technical assistance and to Mrs. Lise-Lotte Jespersen for preparing the *A.v.* PCu protein. The 750 MHz spectra were obtained at The Danish Instrument Center for NMR Spectroscopy of Biological Macromolecules.

SUPPORTING INFORMATION AVAILABLE

Tables of the ^{15}N, ^{13}C, and revised ^{1}H chemical shifts, the relaxation rates R_1 and R_2, the NOE data, and the model-free parameters of *A.v.* plastocyanin. This material is available free of charge via the Internet at http://pubs.acs.org.

REFERENCES

1. Kay, L. E. (1998) *Nat. Struct. Biol. 5*, 513−517.
2. Feher, V. A., and Cavanagh, J. (1999) *Nature 400*, 289−293.
3. Volkman, B. F., Lipson, D., Wemmer, D. E., and Kern, D. (2001) *Science 291*, 2429−2433.
4. Eisenmesser, E. Z., Bosco, D. A., Akke, M., and Kern, D. (2002) *Science 295*, 1520−1523.
5. Kristensen, S. M., Siegal, G., Sankar, A., and Driscoll, P. C. (2000) *J. Mol. Biol. 299*, 771−788.
6. Kasimova, M. R., Kristensen, S. M., Howe, P. W. A., Christensen, T., Matthiesen, F., Petersen, J., Sørensen, H. H., and Led, J. J. (2002) *J. Mol. Biol. 318*, 679−695.
7. Kay, L. E., Torchia, D., and Bax, A. (1989) *Biochemistry 28*, 8972−8979.
8. Farrow, N. A., Muhandiram, R., Singer, A. U., Pascal, S. M., Kay, C. M., Gish, G., Shoelson, S. E., Pawson, T., Forman-Kay, J. D., and Kay, L. E. (1994) *Biochemistry 33*, 5984−6003.
9. Peng, J. W., and Wagner, G. (1992) *Biochemistry 31*, 8571−8586.
10. Palmer, A. G. (1997) *Curr. Opin. Struct. Biol. 7*, 732−737.
11. Kay, L. E. (2001) *Methods Enzymol. 339* (Part B), 174−203.
12. Palmer, A. G., Kroenke, C. D., and Loria, J. P. (2001) *Methods Enzymol. 339* (Part B), 204−238.
13. Mayo, K. H., Daragan, V. A., Idiyatullin, D., and Nesmelova, I. (2000) *J. Magn. Reson. 146*, 188−195.
14. Engelke, J., and Rüterjans, H. (1997) *J. Biomol. NMR 9*, 63−78.
15. Lee, L. K., Rance, M., Chazin, J. W., and Palmer, A. G., III (1997) *J. Biomol. NMR 9*, 287−298.
16. Palmer, A. G., Rance, M., and Wright, P. E. (1991) *J. Am. Chem. Soc. 113*, 4371−4380.
17. Mispelter, J., Lefèvre, C., Adjadj, É., Quiniou, É., and Favaudon, V. (1994) *J. Biomol. NMR 5*, 233−244.
18. Hope, A. B. (2000) *Biochim. Biophys. Acta 1456*, 5−26.
19. Sigfridsson, K. (1998) *Photosynth. Res. 57*, 1−28.
20. Navarro, J. A., Hervás, M. J., and De la Rosa, M. A. (1997) *J. Biol. Inorg. Chem. 2*, 11−22.
21. Bond, C. S., Bendall, D. S., Freeman, H. C., Guss, J. M., Howe, C. J., Wagner, M. J., and Wilce, M. C. (1999) *Acta Crystallogr. D55*, 414−421.
22. Inoue, T., Sugawara, H., Hamanaka, S., Tsukui, H., Suzuki, E., Kohzuma, T., and Kai, Y. (1999) *Biochemistry 38*, 6063−6069.
23. Bertini, I., Ciurli, S., Dikiy, A., Fernàndez, C. O., Luchinat, C., Safarov, N., Shumilin, S., and Vila, A. J. (2001) *J. Am. Chem. Soc. 123*, 2405−2413.
24. Babu, C. R., Volkman, B. F., and Bullerjahn, G. S. (1999) *Biochemistry 38*, 4988−4995.
25. Badsberg, U., Jørgensen, A. M. M., Gesmar, H., Led, J. J., Hammerstad, J. M., Jespersen, L. L., and Ulstrup, J. (1996) *Biochemistry 35*, 7021−7031.
26. Ma, L., Jørgensen, A. M. M., Sørensen, G. O., Ulstrup, J., and Led, J. J. (2000) *J. Am. Chem. Soc. 122*, 9473−9485.
27. Ejdebäk, M., Bergkvist, A., Karlsson, B. G., and Ubbink, M. (2000) *Biochemistry 39*, 5022−5027.
28. Illerhaus, J., Altschmied, L., Reichert, J., Zak, E., Herrmann, R. G., and Haehnel, W. (2000) *J. Biol. Chem. 275*, 17590−17595.
29. Meyer, T. E., Zhao, Z. G., Cusanovich, M. A., and Tollin, G. (1993) *Biochemistry 32*, 4552−4559.
30. Ullmann, G. M., Knapp, E. W., and Kostić, N. M. (1997) *J. Am. Chem. Soc. 119*, 42−52.
31. Hippler, M., Reichert, J., Sutter, M., Zak, E., Altschmied, L., Schröer, U., Herrmann, R. G., and Haehnel, W. (1996) *EMBO J. 15*, 6374−6384.
32. Drepper, F., Hippler, M., Nitschke, W., and Haehnel, W. (1996) *Biochemistry 35*, 1282−1295.
33. Sigfridsson, K., Young, S., and Hansson, Ö. (1996) *Biochemistry 35*, 1249−1257.
34. Sigfridsson, K. (1997) *Photosynth. Res. 54*, 143−153.
35. Young, S., Sigfridsson, K., Olesen, K., and Hansson, Ö. (1997) *Biochim. Biophys. Acta 1322*, 106−114.
36. Christensen, H. E. M., Conrad, L. S., and Ulstrup, J. (1992) *Acta Chem. Scand. 46*, 508−514.
37. Jackman, M. P., Sinclair-Day, J. D., Sisley, M. J., Sykes, A. G., Denys, L. A., and Wright, P. E. (1987) *J. Am. Chem. Soc. 109*, 6443−6449.
38. Davis, D. J., Krogman, D. W., and San Pieto, A. (1980) *Plant Physiol. 65*, 697−702.
39. Crowley, P. B., Otting, G., Schlarb-Ridley, B. G., Canters, G. W., and Ubbink, M. (2001) *J. Am. Chem. Soc. 123*, 10444−10453.
40. Schlarb-Ridley, B. G., Bendall, D. S., and Howe, C. J. (2002) *Biochemistry 41*, 3279−3285.
41. Hansen, D. F., Hass, M. A. S., Christensen, M., Ulstrup, J., and Led, J. J. Unpublished results.
42. Wagner, M. J., Packer, J. C. L., Howe, C. J., and Bendall, D. S. (1996) *Biochim. Biophys. Acta 1276*, 246−252.
43. Bax, A., and Grzesiek, S. (1993) *Acc. Chem. Res. 26*, 131−138.
44. Kay, L. E. (1995) *Prog. Biophys. Mol. Biol. 63*, 277−299.
45. Marion, D., Driscoll, P. C., Kay, L. E., Wingfield, P. T., Bax, A., Gronenborn, A. M., and Clore, G. M. (1989) *Biochemistry 28*, 6150−6156.
46. Cavanagh, J., and Rance, M. (1990) *J. Magn. Reson. 88*, 72−85.
47. Wilker, W., Leibfritz, D., Kerssebaum, R., and Bermel, W. (1993) *Magn. Reson. Chem. 31*, 287−292.

48. Wagner, G., and Brühwiler, D. (1986) *Biochemistry 25*, 5839−5843.
49. Kessler, H., Schmieder, P., and Bermel, W. (1990) *Biopolymers 30*, 465−475.
50. Ikura, M., Kay, L. E., and Bax, A. (1990) *Biochemistry 29*, 4659−4667.
51. Grzesiek, S., and Bax, A. (1992) *J. Magn. Reson. 96*, 432−440.
52. Muhandiram, D. R., and Kay, L. E. (1994) *J. Magn. Reson., Ser. B 103*, 203−216.
53. Kristensen, S. M., Sørensen, M. D., and Led, J. J. (1995) *J. Biomol. NMR 5*, 411−414.
54. States, D. J., Haberkorn, R. A., and Ruben, D. J. (1982) *J. Magn. Reson. 48*, 286−292.
55. Shaka, A. J., Keeler, J., Frenkiel, T., and Freeman, R. (1983) *J. Magn. Reson. 52*, 335−338.
56. Meiboom, S., and Gill, D. (1958) *Rev. Sci. Instrum. 29*, 688−691.
57. Markley, J. L., Hornsley, J. W., and Klein, M. P. (1971) *J. Chem. Phys. 55*, 3604−3605.
58. Delagio, F., Grzesiek, S., Vuister, G. W., Zhu, G., Pfeifer, J., and Bax, A. (1995) *J. Biomol. NMR 6*, 277−293.
59. Gesmar, H., Nielsen, P. F., and Led, J. J. (1994) *J. Magn. Reson., Ser. B 103*, 10−18.
60. Kristensen, S. M., Sørensen, M. D., Gesmar, H., and Led, J. J. (1996) *J. Magn. Reson., Ser. B 112*, 193−196.
61. Mandel, A. M., Akke, M., and Palmer, A. G., III (1995) *J. Mol. Biol. 246*, 141−163.
62. Kay, L. E., Muhandiram, D. R., Wolf, G., Shoelson, S. E., and Forman-Kay, J. D. (1998) *Nat. Struct. Biol. 5*, 156−163.
63. Tjandra, N., Kuboniwa, H., Ren, H., and Bax, A. (1995) *Eur. J. Biochem. 230*, 1014−1024.
64. Tjandra, N., Wingfield, P., Stahl, S., and Bax, A. (1996) *J. Biomol. NMR 8*, 273−284.
65. Lipari, G., and Szabo, A. (1982) *J. Am. Chem. Soc. 104*, 4546−4559.
66. Lipari, G., and Szabo, A. (1982) *J. Am. Chem. Soc. 104*, 4559−4570.
67. Barbato, G., Ikura, M., Kay, L. E., Pastor, R. W., and Bax, A. (1992) *Biochemistry 31*, 5269−5278.
68. Mandel, A. M., Akke, M., and Palmer, A. G., III (1996) *Biochemistry 35*, 16009−16023.
69. Wishart, D. S., and Sykes, B. D. (1994) *Methods Enzymol. 239*, 363−392.
70. Ma, L. (2000) Ph.D. Thesis, University of Copenhagen, Copenhagen, Denmark.
71. Ma, L., Philipp, E., and Led, J. J. (2001) *J. Biomol. NMR 19*, 199−208.
72. Thompson, G. S., Leung, Y.-C., Ferguson, S. J., Radford, S. E., and Redfield, C. (2000) *Protein Sci. 9*, 846−858.
73. Bertini, I., Bryant, D. A., Ciurli, S., Dikiy, A., Fernàndez, C. O., Luchinat, C., Safarov, N., Vila, A. J., and Zhao, J. (2001) *J. Biol. Chem. 276*, 47217−47226.
74. Kojiro, C. L., and Markley, J. L. (1983) *FEBS Lett. 162*, 52−56.
75. Malmström, B. G. (1994) *Eur. J. Biochem. 223*, 711−718.
76. Inoue, T., Gotowada, M., Sugawara, H., Kohzuma, T., Yoshizaki, F., Sugimura, Y., and Kai, Y. (1999) *Biochemistry 38*, 13853−13861.
77. Molina-Heredia, F. P., Hervás, M. J., Navarro, J. A., Dıaz, A., and De la Rosa, M. A. (2001) *J. Biol. Chem. 276*, 601−605.
78. Shibata, N., Inoue, T., Nagano, C., Nishio, N., Kohzuma, T., Onodera, K., Yoshizaki, F., Sugimura, Y., and Kai, Y. (1999) *J. Biol. Chem. 274*, 4225−4230.
79. Kalverda, A. P., Ubbink, M., Gilardi, G., Wijmenga, S., Crawford, A., Jeuken, L. J. C., and Canters, G. W. (1999) *Biochemistry 38*, 12690−12697.
80. Millet, O., Loria, J. P., Kroenke, C. D., Pons, M., and Palmer, A. G., III (2000) *J. Am. Chem. Soc. 122*, 2867−2877.
81. Stone, M. J., Chandrasekhar, K., Holmgren, A., Wright, P. E., and Dyson, H. J. (1993) *Biochemistry 32*, 426−435.
82. LeMaster, D. M., and Kushlan, D. M. (1996) *J. Am. Chem. Soc. 118*, 9255−9264.

BI020553H